

Modulation of Mammalian Inositol 1,4,5-Trisphosphate Receptor Isoforms by Calcium: A Role of Calcium Sensor Region

Huiping Tu, Zhengnan Wang, and Ilya Bezprozvanny

Department of Physiology, University of Texas Southwestern Medical Center at Dallas, Dallas, Texas 75390

ABSTRACT In the accompanying article, we compared main functional properties of the three mammalian inositol 1,4,5-trisphosphate receptors (InsP₃R) isoforms. In this article we focused on modulation of mammalian InsP₃R isoforms by cytosolic Ca²⁺. We found that: 1), when recorded in the presence of 2 μM InsP₃ and 0.5 mM ATP all three mammalian InsP₃R isoforms display bell-shaped Ca²⁺ dependence in physiological range of Ca²⁺ concentrations (pCa 8–5); 2), in the same experimental conditions InsP₃R3 is most sensitive to modulation by Ca²⁺ (peak at 107 nM Ca²⁺), followed by InsP₃R2 (peak at 154 nM Ca²⁺), and then by InsP₃R1 (peak at 257 nM Ca²⁺); 3), increase in ATP concentration to 5 mM had no significant effect of Ca²⁺ dependence of InsP₃R1 and InsP₃R2; 4), increase in ATP concentration to 5 mM converted Ca²⁺ dependence of InsP₃R3 from “narrow” shape to “square” shape; 5), ATP-induced change in the shape of InsP₃R3 Ca²⁺ dependence was mainly due to an >200-fold reduction in the apparent affinity of the Ca²⁺-inhibitory site; 6), the apparent Ca²⁺ affinity of the Ca²⁺ sensor region (Cas) determined in biochemical experiments is equal to 0.23 μM Ca²⁺ for RT1-Cas, 0.16 μM Ca²⁺ for RT2-Cas, and 0.10 μM Ca²⁺ for RT3-Cas; and 7), Ca²⁺ sensitivity of InsP₃R1 and InsP₃R3 isoforms recorded in the presence of 2 μM InsP₃ and 0.5 mM ATP or 2 μM InsP₃ and 5 mM ATP can be exchanged by swapping their Cas regions. Obtained results provide novel information about functional properties of mammalian InsP₃R isoforms and support the importance of the Ca²⁺ sensor region (Cas) in determining the sensitivity of InsP₃R isoforms to modulation by Ca²⁺.

INTRODUCTION

The inositol (1,4,5)-trisphosphate receptor (InsP₃R) is an intracellular calcium (Ca²⁺) release channel that plays a key role in Ca²⁺ signaling in cells (Berridge, 1993). Three mammalian InsP₃R isoforms—InsP₃R type 1 (InsP₃R1), InsP₃R type 2 (InsP₃R2), and InsP₃R type 3 (InsP₃R3)—are expressed in mammals (Furuichi et al., 1994), each with the unique expression pattern (Taylor et al., 1999). Modulation of InsP₃R by cytosolic Ca²⁺ is one of the most fundamental InsP₃R properties responsible for complex spatiotemporal aspects of Ca²⁺ signaling (Berridge, 1993). In the accompanying article (Tu et al., 2005), we used the planar lipid bilayer reconstitution technique to compare main functional properties (conductance, gating, InsP₃ sensitivity, and modulation by ATP) of the recombinant rat InsP₃R1, InsP₃R2, and InsP₃R3 expressed in Sf9 cells by baculoviral infection. In this article, we used the planar lipid bilayer reconstitution technique and biochemical experiments to compare modulation of mammalian InsP₃R isoforms by cytosolic Ca²⁺. In our previous studies, we identified a putative Ca²⁺ sensor region (Cas) within a modulatory domain of InsP₃R1 (Miyakawa et al., 2001; Tu et al., 2003). Here we show that the observed differences in Ca²⁺ sensitivity between mammalian InsP₃R isoforms can be explained by isoform-specific differences in affinities of the Cas region

for Ca²⁺. Our results provide information about Ca²⁺ modulation of three mammalian InsP₃R isoforms and further support a role of the Ca²⁺ sensor region (Cas) in the InsP₃R modulation by Ca²⁺.

MATERIAL AND METHODS

Generation of recombinant baculoviruses

The baculoviruses expressing rat InsP₃R1 (RT1) and rat InsP₃R3 (RT3) have been previously described (Maes et al., 2000; Tu et al., 2002). The generation of baculovirus encoding rat InsP₃R2 (RT2) is described in the accompanying article (Tu et al., 2005). The RT1-V-3 and RT3-V-1 chimeric constructs in pFastBac1 vector (Invitrogen, Carlsbad, CA) were generated by PCR-mediated gene fusion and verified by sequencing. In RT1-V-3 construct amino acids E1932-L2312 of InsP₃R1 were replaced with amino acids M1835-F2242 of InsP₃R3; in RT3-V-1 construct amino acids M1835-F2242 of InsP₃R3 were replaced with amino acids E1932-L2312 of InsP₃R1. The RT1-V-3 and RT3-V-1 baculoviruses were generated and amplified using Bac-to-Bac system according to the manufacturer's (Invitrogen) instructions. Expression of RT1-V-3 and RT3-V-1 proteins in Sf9 cells was confirmed by Western blotting with rabbit polyclonal anti-InsP₃R1 antibody T443 described previously (Kaznacheyeva et al., 1998) and the affinity purified rabbit polyclonal anti-InsP₃R3 antibody (IB7124-AP) described in the accompanying article (Tu et al., 2005).

Expression of InsP₃R in Sf9 cells and planar lipid bilayer experiments

RT1, RT2, RT3 isoforms, RT1-V-3, and RT3-V-1 chimeras were expressed in Sf9 cells and reconstituted into planar lipid bilayers as described in the accompanying article (Tu et al., 2005). Single-channel analysis of currents supported by RT1-V-3 and RT3-V-1 chimeras was performed as described for RT1, RT2, and RT3 isoforms in the accompanying article (Tu et al., 2005). Ca²⁺ dependence of InsP₃R isoforms and chimeras was determined

Submitted July 14, 2004, and accepted for publication October 29, 2004.

Address reprint requests to Dr. Ilya Bezprozvanny, Dept. of Physiology, K4.112 UT Southwestern Medical Center at Dallas, 5323 Harry Hines Blvd., Dallas, TX 75390-9040. Tel.: 214-648-6737; Fax: 214-648-2974; E-mail: ilya.bezprozvanny@utsouthwestern.edu.

© 2005 by the Biophysical Society

0006-3495/05/02/1056/14 \$2.00

doi: 10.1529/biophysj.104.049601

as described in Bezprozvanny et al. (1991) by consecutive additions CaCl₂ to the *cis* (cytosolic) chamber from the concentrated 20 mM CaCl₂ stock with at least 30 s stirring of solutions in both chambers. Calcium concentration in 20 mM CaCl₂ stock solution was verified by atomic absorption spectroscopy (Galbraith Laboratories, Knoxville, TN). Free Ca²⁺ concentration in the *cis* chamber was controlled in the range from 10 nM Ca²⁺ (pCa 8) to 100 μM Ca²⁺ (pCa 4) by the mixture of 1 mM EGTA, 1 mM HEDTA, and variable concentrations of CaCl₂ and calculated by using a program described in Fabiato (1988). Evidence for the presence of multiple channels in the bilayer (multiple open levels) was obtained in the majority of the experiments. The single-channel open probability (*Po*) was estimated from multichannel records and normalized to the maximum *Po* observed in the same experiment as described for InsP₃- and ATP-dependence experiments in the accompanying article (Tu et al., 2005). The normalized data from several experiments with each InsP₃R isoform or chimera were averaged together for presentation and fitting as described for InsP₃- and ATP-dependence experiments in the accompanying article (Tu et al., 2005).

To obtain parameters of Ca²⁺ dependence the normalized and averaged data were fit by the “bell-shaped equation”:

$$P(\text{Ca}^{2+}) = 4P_m k_{\text{Ca}}^n [\text{Ca}^{2+}]^n / ((k_{\text{Ca}}^n + [\text{Ca}^{2+}]^n)(K_{\text{Ca}}^n + [\text{Ca}^{2+}]^n)), \quad (1)$$

modified from Bezprozvanny et al. (1991), where P_m is a parameter proportional to the maximal normalized *Po* value, n is the Hill coefficient, K_{Ca} is the apparent affinity of the Ca²⁺-activating site, and k_{Ca} is the apparent affinity of the Ca²⁺-inhibitory site. As explained in Tu et al. (2003), parameter P_m is equal to maximal normalized *Po* only in the case when $k_{\text{Ca}} = K_{\text{Ca}}$. If $k_{\text{Ca}} \neq K_{\text{Ca}}$, parameter *Po* is proportional (and higher) than maximal *Po*.

To obtain parameters of Ca²⁺ dependence of InsP₃R3 and RT1-V-3 at 5 mM ATP, the normalized and averaged data were fit by the “biphasic Hill equation”:

$$P(\text{Ca}^{2+}) = P_m / ((1 + (K_{\text{Ca}}/[\text{Ca}^{2+}])^{\text{Ha}})(1 + ([\text{Ca}^{2+}]/k_{\text{Ca}})^{\text{Hi}})), \quad (2)$$

modified from Mak et al. (1998), where P_m is a parameter proportional to the maximal normalized *Po* value, *Ha* is the Hill coefficient of the activation phase, K_{Ca} is the apparent affinity of the Ca²⁺-activating site, *Hi* is the Hill coefficient of the inhibitory phase, and k_{Ca} is the apparent affinity of the Ca²⁺-inhibitory site.

The fits using Eqs. 1 and 2 were generated using least-squares routine (Sigma Plot 2001, Jandel Scientific) and the quality of the fit was evaluated from the coefficient of determination (*R*²). The standard errors of resulting parameters were obtained as the estimates of the uncertainties in the values of regression coefficients obtained as a result of the fitting procedure (Sigma Plot 2001, Jandel Scientific, San Rafael, CA).

Ca²⁺ binding assay

RT1-Cas (E1932-R2270 of rat InsP₃R1) expression construct in pGEX-KG expression vector (Amersham-Pharmacia Biotech, Uppsala, Sweden) was previously described (Tu et al., 2003). RT2-Cas (E1884-R2224 of rat InsP₃R2) and RT3-Cas (M1835-R2199 of rat InsP₃R3) regions were amplified by polymerase chain reaction (PCR) and subcloned into pGEX-KG vector. RT1-Cas, RT2-Cas, and RT3-Cas proteins were expressed in BL21 bacteria, purified on glutathione-sepharose 4B beads (Amersham-Pharmacia Biotech), and cleaved from glutathione *S*-transferase (GST) by thrombin as previously described for RT1-Cas (Tu et al., 2003). Obtained proteins were used immediately in intrinsic tryptophan fluorescence spectroscopy measurements performed as previously described for RT1-Cas (Tu et al., 2003). Briefly, a quartz cuvette containing 2 ml of recombinant proteins at 80 μg/ml in *cis* recording buffer (110 mM Tris dissolved in HEPES, pH 7.35) was supplemented with 1 mM EGTA and

1 mM HEDTA (pH 7.35). The free Ca²⁺ concentration in the cuvette was adjusted in the range pCa 9.4–2 by consecutive additions of calibrated CaCl₂ stock solutions (20 mM CaCl₂, 100 mM CaCl₂, and 1 M CaCl₂) with constant stirring. The free Ca²⁺ concentration in the cuvette was calculated using MaxChelator (<http://www.stanford.edu/~cpatton/maxc.html>). Intrinsic tryptophan fluorescence was excited by 280 nm (2-nm-slit width) light (DeltaRAM, Photon Technology International, Lawrenceville, NJ) and emission spectra were collected at room temperature in the 290–500-nm range with a 2-nm step size. The experiments were controlled and analyzed by Felix software package (Photon Technology International).

The absolute peak tryptophan fluorescence values at each Ca²⁺ concentration $F(\text{Ca}^{2+})$ were determined from the generated emission spectra. The measured peak fluorescence values were corrected for dilution $F_{\text{cor}}(\text{Ca}^{2+}) = F_0/(1 + v/V)$, where $F_{\text{cor}}(\text{Ca}^{2+})$ is dilution-corrected peak fluorescence value, F_0 is the peak fluorescence value with no CaCl₂ added (pCa 9.4), v is the total volume of CaCl₂ added, and V is the starting solution volume in the cuvette (2 ml). The difference between measured and dilution-corrected peak tryptophan fluorescence values $\Delta F(\text{Ca}^{2+}) = F(\text{Ca}^{2+}) - F_{\text{cor}}(\text{Ca}^{2+})$ was taken as a measure of Ca²⁺-induced conformational changes in RT1-Cas, RT2-Cas, and RT3-Cas recombinant proteins (Tu et al., 2003; Ward, 1985). The ΔF values at each Ca²⁺ concentration were normalized to the maximal ΔF value (ΔF_{max}) measured at pCa 2.0 in the same experiment. The normalized ΔF values from three independent experiments for each recombinant protein were averaged together at each Ca²⁺ concentration for presentation and fitting. The Ca²⁺ dependence of the normalized and averaged ΔF values was fit using equation

$$\Delta F/\Delta F_{\text{max}}(\text{Ca}^{2+}) = [\text{Ca}^{2+}]^n / ([\text{Ca}^{2+}]^n + K_{\text{Ca}}^n), \quad (3)$$

from Tu et al. (2003), where $[\text{Ca}^{2+}]$ is the Ca²⁺ concentration in the cuvette, n is the Hill coefficient, and K_{Ca} is the apparent affinity for Ca²⁺. The fits were generated using least-squares routine (Sigma Plot 2001, Jandel Scientific), and the quality of the fit was evaluated from the coefficient of determination (*R*²). The standard errors of resulting K_{Ca} and n values were obtained as the estimates of the uncertainties in the values of regression coefficients obtained as a result of the fitting procedure (Sigma Plot 2001, Jandel Scientific).

RESULTS

Modulation of mammalian InsP₃R isoforms by Ca²⁺

In the accompanying article (Tu et al., 2005), we compared main functional properties (conductance, gating, InsP₃ sensitivity, and modulation by ATP) of the recombinant rat InsP₃R1, InsP₃R2, and InsP₃R3 expressed in Sf9 cells by baculoviral infection and reconstituted into planar lipid bilayers. Modulation of InsP₃R by cytosolic Ca²⁺ is one of the most fundamental InsP₃R properties responsible for complex spatiotemporal aspects of Ca²⁺ signaling (Berridge, 1993). Does cytosolic Ca²⁺ affect InsP₃R function in an isoform-specific manner? To answer this question we determined Ca²⁺ dependence of recombinant InsP₃R1, InsP₃R2, and InsP₃R3 in the presence of 2 μM InsP₃ and 0.5 mM ATP. Because most of the experiments resulted in multichannel bilayers, the *Po* values in each experiment were normalized to the maximal *Po* in the same experiment as described in Materials and Methods, and the normalized data from different experiments with each InsP₃R isoform were averaged together for presentation and analysis. In agreement with our previous findings (Nosyreva et al., 2002; Tu

et al., 2002, 2003), InsP₃R1 expressed in Sf9 cells (RT1) display bell-shaped Ca²⁺ dependence with the peak at 257 nM Ca²⁺ (Fig. 1, *open circles*). Fit to the RT1 Ca²⁺ dependence using Eq. 1 (Fig. 1, *curve*; $R^2 = 0.99$) yielded apparent affinities of activating (K_{Ca}) and inhibitory (k_{Ca}) sites equal to $0.17 \pm 0.03 \mu\text{M Ca}^{2+}$ and $0.37 \pm 0.01 \mu\text{M Ca}^{2+}$, respectively (Table 1). Similar to RT1, RT2 and RT3 also displayed bell-shaped Ca²⁺ dependence in the physiological range of Ca²⁺ concentrations (pCa 8–5). The peak of bell-shaped Ca²⁺ dependence was located at 154 nM Ca²⁺ for RT2 (Fig. 1, *solid triangles*), and at 107 nM Ca²⁺ for RT3 (Fig. 1, *solid circles*). Fit to the RT2 and RT3 Ca²⁺ dependence using Eq. 1 (Fig. 1, *curves*; $R^2 = 0.98$ for RT2 and $R^2 = 0.94$ for RT3) yielded the apparent affinities of the activating and inhibitory sites equal to $0.15 \pm 0.04 \mu\text{M Ca}^{2+}$ and $0.16 \pm 0.04 \mu\text{M Ca}^{2+}$ for RT2, and $0.06 \pm 0.03 \mu\text{M Ca}^{2+}$ and $0.17 \pm 0.02 \mu\text{M Ca}^{2+}$ for RT3, respectively (Table 1).

As described in the accompanying article (Tu et al., 2005), 5 mM concentration of ATP is required to maximally activate RT3 channels. Thus, in the next series of experiments we determined Ca²⁺ dependence of RT3 in the presence of 2 $\mu\text{M InsP}_3$ and 5 mM ATP. We found that in the presence of 5 mM ATP, RT3 displayed a “square-shaped” Ca²⁺ dependence with the maximal channel activity observed in the range of Ca²⁺ concentrations between 0.1 $\mu\text{M Ca}^{2+}$ and 10 $\mu\text{M Ca}^{2+}$ (pCa 7–5) (Fig. 2, *solid circles*). The “square-shaped” Ca²⁺ dependence observed in this condition is similar to “square-shaped” Ca²⁺ dependence described for *Xenopus* InsP₃R (InsP₃R1) (Mak et al., 1998) and rat InsP₃R3 expressed in *Xenopus* oocytes (Mak et al., 2001b). Thus, to fit these data we used “biphasic Hill equation” (Eq. 2) adapted from Mak et al. (1998). Fit to RT3 Ca²⁺-dependence data using Eq. 2 (Fig. 2, *thick curve*; $R^2 = 0.93$) yielded apparent affinities of activating and inhibitory sites equal to $0.029 \pm 0.004 \mu\text{M Ca}^{2+}$ and $37 \pm 6 \mu\text{M Ca}^{2+}$

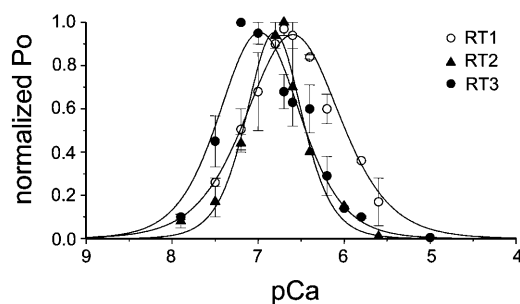


FIGURE 1 Ca²⁺ dependence of mammalian InsP₃R isoforms. The single-channel open probability (P_o) for each InsP₃R isoform was measured as a function of cytosolic Ca²⁺ concentrations from 10 nM to 5 $\mu\text{M Ca}^{2+}$ on the *cis* (cytoplasmic) side of the membrane in the presence of 2 $\mu\text{M InsP}_3$ and 0.5 mM Na₂ATP. The normalized and averaged data (see Materials and Methods) at each Ca²⁺ concentration are shown as means \pm SE ($n \geq 3$) for RT1 (\circ), RT2 (\blacktriangle), RT3 (\bullet). These data were fitted by Eq. 1 (see Materials and Methods). The parameters of the best fit (*curves*) are in Table 1.

(Table 1). Thus, increase in ATP concentration to 5 mM had only a twofold effect on the apparent affinity of the Ca²⁺-activating site of InsP₃R3, but resulted in a >200-fold reduction in the apparent affinity of the Ca²⁺-inhibitory site of InsP₃R3 (Table 1). In contrast to InsP₃R3 (Fig. 2), we found that the Ca²⁺ dependence of InsP₃R1 and InsP₃R2 was not significantly different at 0.5 mM ATP and at 5 mM ATP (data not shown).

Ca²⁺ binding to InsP₃R Ca²⁺ sensor

Different Ca²⁺ sensitivity of InsP₃R1, InsP₃R2, and InsP₃R3 has been observed in our experiments performed at 2 $\mu\text{M InsP}_3$ and 0.5 mM ATP (Fig. 1; Table 1). We previously proposed that the putative Ca²⁺ sensor region (Cas) in the coupling domain of InsP₃R1 is responsible for InsP₃R1 modulation by Ca²⁺ (Miyakawa et al., 2001; Tu et al., 2003). If “Ca²⁺ sensor hypothesis” is correct, then the differences in Ca²⁺ sensitivity between InsP₃R isoforms should correlate with the differences in Ca²⁺ affinities of corresponding Cas regions. To test this prediction, we expressed in bacteria and purified RT1-Cas (E1932-R2270 of rat InsP₃R1), RT2-Cas (E1884-R2224 of rat InsP₃R2), and RT3-Cas (M1835-R2199 of rat InsP₃R3) proteins (Fig. 3 A). Similar yield of RT-Cas proteins was obtained as a result of our expression and purification procedure for each InsP₃R isoform (Fig. 3 B).

Sequence alignment of RT1-Cas, RT2-Cas, and RT3-Cas regions shows a high degree of sequence conservation (Fig. 4). The E2100 glutamate residue that we previously identified to be critical for InsP₃R1 modulation by Ca²⁺ (Miyakawa et al., 2001; Tu et al., 2003) is conserved in InsP₃R2 (E2053) and InsP₃R3 (E2004) sequences (Fig. 4, *arrow*). In the previous study (Tu et al., 2003), we utilized intrinsic tryptophan fluorescence assay to compare Ca²⁺ binding affinity of RT1-Cas wild type and E2100 mutants. The W2255 and W2267 residues of InsP₃R1 present within the RT1-Cas region (Fig. 4, *open arrows*) are conserved in InsP₃R2 (W2209 and W2221) and in InsP₃R3 (W2183 and W2195). For all three InsP₃R isoforms, these are the only two tryptophan residues within Cas sequence (Fig. 4). Thus, we reasoned that intrinsic tryptophan fluorescence of RT2-Cas and RT3-Cas proteins is likely to be quenched in a Ca²⁺-dependent manner similar to our previous findings with RT1-Cas (Tu et al., 2003).

To test this hypothesis, we collected emission spectra (excitation at 280 nm) of RT1-Cas, RT2-Cas, and RT3-Cas proteins at different Ca²⁺ concentrations (pCa 9.4–2.0, buffered by 1 mM EGTA and 1 mM HEDTA). We found that the position of the emission peak (λ_{max}) remained constant at 332 nm for all three RT-Cas proteins at all Ca²⁺ concentrations (Fig. 5, A–C). However, a systematic and saturable change in the intensity of the intrinsic fluorescent signal was observed for all three RT-Cas proteins as a function of Ca²⁺ (Fig. 5, A–C). To compare the data

TABLE 1 Ca²⁺ dependence of mammalian InsP₃R isoforms and Ca²⁺ sensor swap chimeras

InsP ₃ R	Ca ²⁺ dependence					Ca ²⁺ binding	
	ATP (mM)	Activation K_{Ca} (μ M)	Inhibition k_{Ca} (μ M)	Hill coefficient n_{Hill}	Peak (nM Ca ²⁺)	K_{Ca} (μ M)	Hill coefficient n_{Hill}
RT1	0.5	0.17 \pm 0.03	0.37 \pm 0.01	1.23	257	0.23 \pm 0.04	0.47
RT2	0.5	0.15 \pm 0.04	0.16 \pm 0.04	2.05	154	0.16 \pm 0.06	0.37
RT3	0.5	0.06 \pm 0.03	0.17 \pm 0.02	1.46	107	0.10 \pm 0.04	0.39
	5	0.029 \pm 0.004	37 \pm 6	1.80 (<i>Ha</i>) 1.17 (<i>Hi</i>)	100–10,000		
RT1-V-3	0.5	0.06 \pm 0.02	0.16 \pm 0.01	2.17	100	RT3	RT3
	5	0.04 \pm 0.003	33 \pm 5	4.0 (<i>Ha</i>) 1.8 (<i>Hi</i>)	100–10,000		
RT3-V-1	0.5	0.24 \pm 0.01	0.25 \pm 0.02	1.65	239	RT1	RT1
	5	0.28 \pm 0.03	0.31 \pm 0.04	0.94	310		

Entries in the “Ca²⁺ binding” columns for RT1-V-3 and RT3-V-1 chimeras are used to indicate the “parental” InsP₃R isoform for the Cas region in each chimera. Both *Ha* and *Hi* values (see Eq. 2) are entered in the n_{Hill} column for RT3 Ca²⁺ dependence at 5 mM ATP.

from different experiments, the observed changes in RT1-Cas, RT2-Cas, and RT3-Cas peak fluorescence intensity (ΔF) were corrected for dilution (see Materials and Methods), normalized to the maximal change in the peak fluorescence intensity (ΔF_{max}), averaged, and plotted against Ca²⁺ concentration (Fig. 6). By fitting the obtained results using Eq. 3 (see Materials and Methods) (Fig. 6, curves; $R^2 = 1.0$ for RT1-Cas, $R^2 = 0.99$ for RT2-Cas, and $R^2 = 0.98$ for RT3-Cas), we determined that the apparent affinity for Ca²⁺ (K_{Ca}) is equal to 0.23 \pm 0.04 μ M for RT1-Cas, 0.16 \pm 0.06 μ M for RT2-Cas, and 0.10 \pm 0.04 μ M for RT3-Cas (Table 1). Obtained results are in quantitative agreement with the sensitivity of InsP₃R isoforms to Ca²⁺ modulation determined in planar lipid bilayer experiments (Fig. 1; Table 1). For all three RT-Cas regions, the Hill coefficient (n_{Hill}) determined in Ca²⁺-binding experiments was in the range 0.4–0.5 (Fig. 6; Table 1). As discussed previously for RT1-Cas (Tu et al., 2003), an apparent negative cooperativity in association of RT-Cas regions with Ca²⁺ may be due to multimerization of recombinant proteins during our measurements or due to the presence of multiple Ca²⁺ binding sites within the RT-Cas regions.

Functional analysis of InsP₃R Ca²⁺ sensor swap chimeras

Is Cas region alone sufficient to determine InsP₃R sensitivity to Ca²⁺? To answer this question and to further test the “Ca²⁺ sensor hypothesis” (Miyakawa et al., 2001; Tu et al., 2003), we generated chimeric RT1-V-3 and RT3-V-1 baculoviruses by swapping Cas-containing regions between InsP₃R1 and InsP₃R3 (Fig. 7 A). The regions swapped in RT1-V-3 and RT3-V-1 chimeras had the same amino-terminal boundary (E1932 in InsP₃R1 and M1835 in InsP₃R3) as the soluble RT1-Cas and RT3-Cas constructs expressed in bacteria (see Fig. 4). To simplify the construction, the swapped regions were 43 amino acids longer on carboxy-termini than the soluble RT1-Cas and RT3-Cas constructs (to the middle of the second predicted transmembrane domain, L2312 in InsP₃R1 and F2242 of

InsP₃R3) (see Fig. 4). As discussed in the accompanying article (Tu et al., 2005), coupling domain of InsP₃R1 contains high-affinity (ATPA) and low-affinity (ATPB) ATP-binding sites (Fig. 7 A). In contrast, coupling domain of InsP₃R3 contains only low-affinity (ATPB) ATP-binding site (Fig. 7 A). Cas regions of InsP₃R1 and InsP₃R3 include corresponding ATPB sites in their sequence (Fig. 4). Thus, RT1-V-3 chimera contains the high-affinity ATPA site from InsP₃R1 and the low-affinity ATPB site from InsP₃R3 (Fig. 7 A). In contrast, RT3-V-1 chimera contains only the low-affinity ATPB site from InsP₃R1 (Fig. 7 A). As discussed in the accompanying article (Tu et al., 2005), InsP₃R1 and InsP₃R3 differ dramatically in their sensitivity to ATP modulation. Thus, swapping Cas regions may affect not only Ca²⁺, but also ATP dependence of parental constructs. Expression of RT1-V-3 and RT3-V-1 proteins in Sf9 cells was confirmed by Western blotting with anti-InsP₃R1 T443 antibodies (Fig. 7 B) and anti-InsP₃R3 affinity purified IB7124 antibodies (Fig. 7 C). The epitopes for T443 antibodies (Kaznacheyeva et al., 1998) and IB7124 anti-

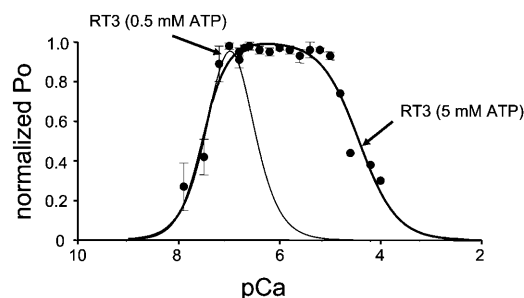


FIGURE 2 Ca²⁺ dependence of InsP₃R3 isoform at 5 mM ATP. The single-channel open probability (P_o) for InsP₃R3 (RT3) was measured as a function of cytosolic Ca²⁺ concentrations from 10 nM to 100 μ M Ca²⁺ on the *cis* (cytoplasmic) side of the membrane in the presence of 2 μ M InsP₃ and 5 mM Na₂ATP. The normalized and averaged data (see Materials and Methods) at each Ca²⁺ concentration are shown as means \pm SE ($n \geq 3$) (●). These data were fit by Eq. 2 (see Materials and Methods). The parameters of the best fit (thick line) are in Table 1. The fit to the RT3 Ca²⁺ dependence in the presence of 2 μ M InsP₃ and 0.5 mM Na₂ATP (thin line) is from Fig. 1.

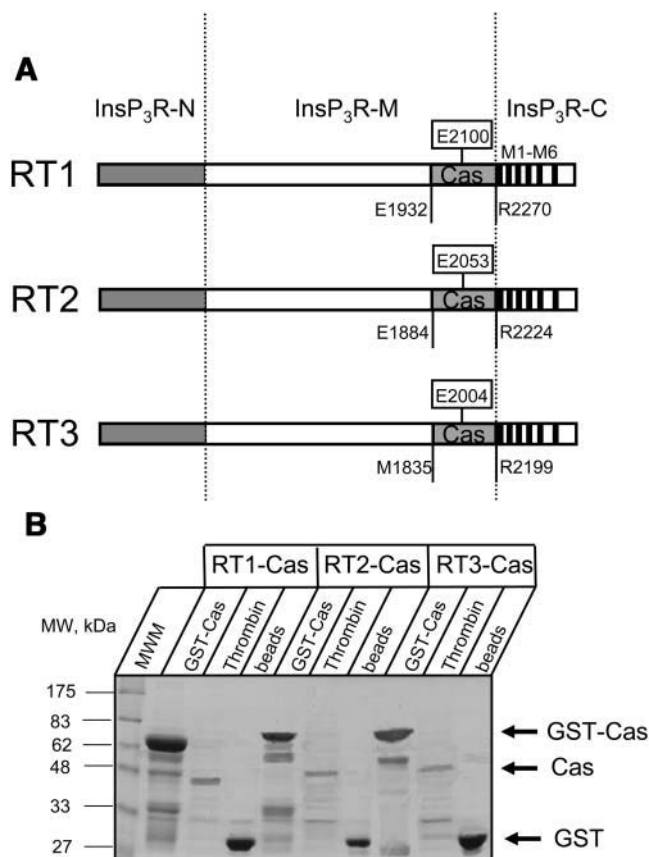


FIGURE 3 Expression and purification of the putative Ca^{2+} sensor (Cas) regions of mammalian InsP_3R isoforms (adapted from Furuichi et al., 1994). The boundaries of the amino-terminal InsP_3 binding domain $\text{InsP}_3\text{R-N}$, the carboxyl-terminal channel-forming domain $\text{InsP}_3\text{R-C}$ with transmembrane domains M1–M6, and the middle coupling domain $\text{InsP}_3\text{R-M}$ are indicated. The putative InsP_3R Ca^{2+} sensor region (Cas) is shown for $\text{InsP}_3\text{R1}$ (E1932–R2270), $\text{InsP}_3\text{R2}$ (E1884–R2224), and $\text{InsP}_3\text{R3}$ (M1835–R2199). (B) Expression and purification of the putative Ca^{2+} sensor (Cas) regions of mammalian InsP_3R isoforms. Samples of GST-Cas attached to glutathione beads (GST-Cas), Cas proteins released by thrombin cleavage (Thrombin), and glutathione beads after thrombin cleavage (beads) were analyzed by SDS-PAGE gel electrophoresis (10% polyacrylamide gel stained with Coomassie blue). The predicted molecular weight of GST-Cas (68 kDa), Cas (39 kDa), and GST (29 kDa) are indicated by the arrows. Total protein of 1/60 (GST-Cas and beads lanes) or 1/200 (Thrombin lanes) was loaded on the gel for RT1-Cas, RT2-Cas, and RT3-Cas.

bodies (Tu et al., 2005) are located at the carboxy-terminal ends of $\text{InsP}_3\text{R1}$ and $\text{InsP}_3\text{R3}$ sequences, which are not affected by swapping Cas-containing domains in RT1-V-3 and RT3-V-1 chimeras (Fig. 7 A).

Recombinant RT1-V-3 and RT3-V-1 chimeric proteins formed functional InsP_3 -gated channels in planar lipid bilayers when recorded in standard recording conditions (pCa 6.7, 0.5 mM ATP, 2 μM InsP_3) (Figs. 8 A and 9 A). The Gaussian fit to the amplitude histogram of currents supported by RT1-V-3 chimera (Fig. 8 B) resulted in the average unitary current amplitude of RT1-V-3 channels equal to 1.86

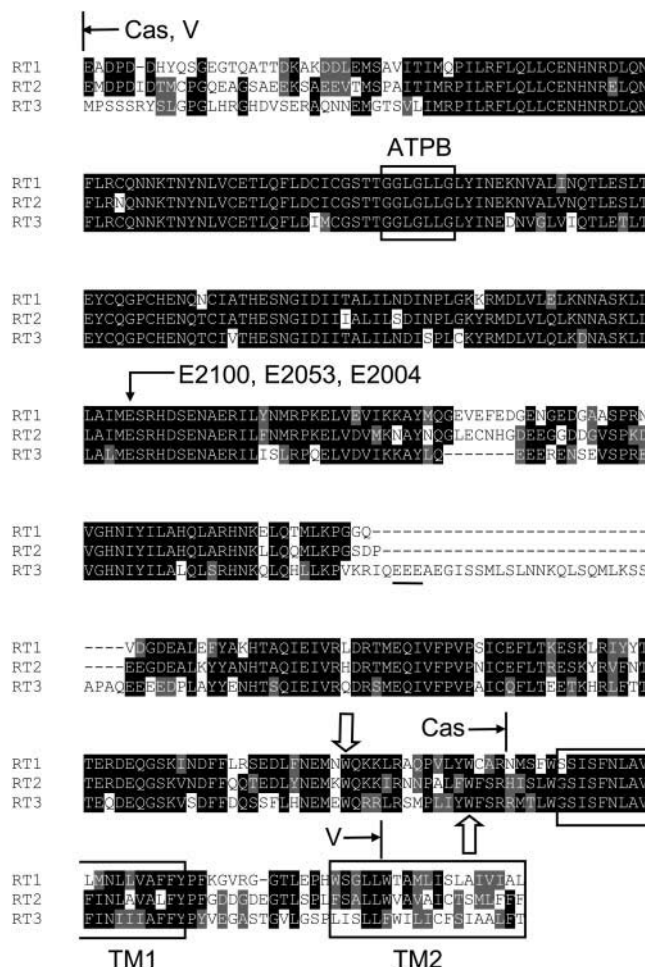


FIGURE 4 Sequence alignment of InsP_3R Cas regions. The fragment of rat $\text{InsP}_3\text{R1}$ sequence (P29994, E1932–L2326) is aligned with the corresponding region of rat $\text{InsP}_3\text{R2}$ (P29995, E1884–F2281) and rat $\text{InsP}_3\text{R3}$ (Q63269, M1825–T2255). The amino-terminal boundary of the alignment (E1932 in $\text{InsP}_3\text{R1}$) is chosen from the limited trypsin digestion pattern of $\text{InsP}_3\text{R1}$ (Yoshikawa et al., 1999). The carboxy-terminal boundary of the alignment (L2326 in $\text{InsP}_3\text{R1}$) corresponds to the end of the predicted second transmembrane domain (TM2). The boundaries of soluble RT-Cas constructs (Cas) and the domain swap boundaries in RT1-V-3 and RT3-V-1 chimeras (V) are shown. Also shown is the ATPB binding site (²⁰¹⁵GGLGLLG²⁰²¹ in $\text{InsP}_3\text{R1}$) (Maes et al., 2001), conserved glutamate residue (E2100 in $\text{InsP}_3\text{R1}$) mutated in our previous studies of $\text{InsP}_3\text{R1}$ Ca^{2+} sensor (Miyakawa et al., 2001; Tu et al., 2003), two conserved tryptophan residues (W2255 and W2267 in $\text{InsP}_3\text{R1}$) present within the RT-Cas region, a unique EEE cluster in the RT3-Cas sequence, and predicted boundaries of the TM1 and TM2 transmembrane domains.

± 0.06 pA ($n = 3$) and the mean P_o of RT1-V-3 channels equal to $20 \pm 4\%$ ($n = 3$). The open and closed dwell time distributions of RT1-V-3 channels could be fit with a single exponential function (Fig. 8, C and D) that yielded the mean open time of RT1-V-3 channels equal to 7.8 ± 0.9 ms ($n = 3$) and the mean closed time of RT1-V-3 channels equal to 10 ± 1 ms ($n = 3$). The Gaussian fit to the amplitude histogram of currents supported by RT3-V-1 chimera (Fig. 9 B) yielded the average unitary current amplitude equal to

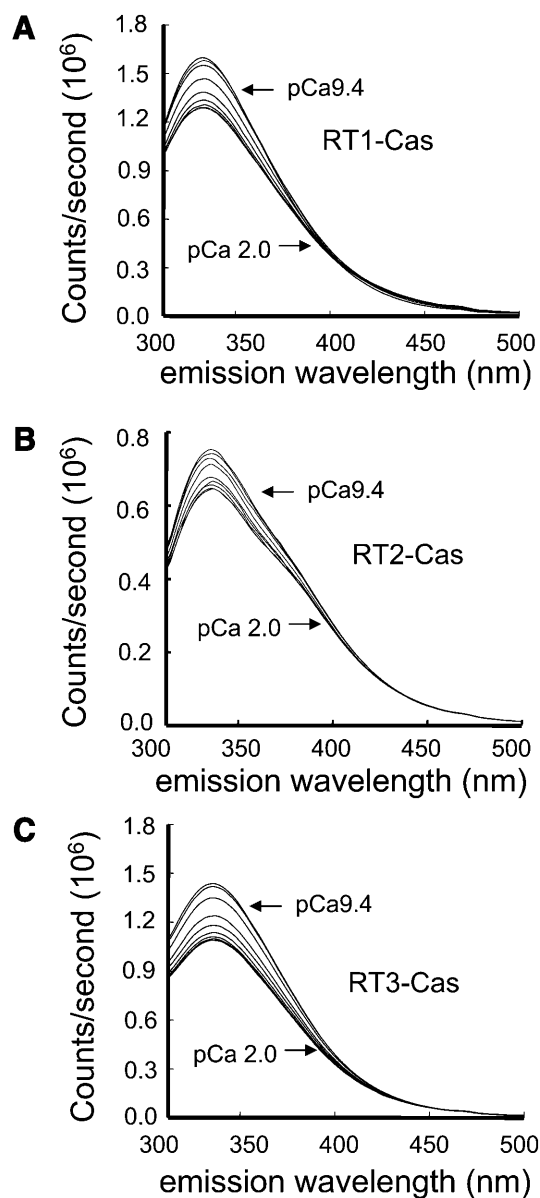


FIGURE 5 Intrinsic tryptophan fluorescence emission spectra of the InsP₃R Ca²⁺ sensor region. Representative intrinsic tryptophan fluorescence emission spectra of RT1-Cas (A), RT2-Cas (B), and RT3-Cas (C) proteins at variable Ca²⁺ concentrations (pCa 9.4–2.0, as indicated). Similar results were obtained in at least three independent experiments with RT1-Cas, RT2-Cas, and RT3-Cas proteins.

1.87 ± 0.06 pA ($n = 3$) and the mean P_o equal to $8 \pm 3\%$ ($n = 3$). The open dwell time and closed dwell time distributions of RT3-V-1 currents were fit by a single exponential function (Fig. 9, C and D), resulting in the mean open time of RT3-V-1 channels equal to 8 ± 1 ms ($n = 3$) and the mean closed time equal to 83 ± 5 ms ($n = 3$). Thus, conductance and gating properties of RT1-V-3 and RT3-V-1 chimeric channels are similar to conductance and gating properties of wild-type InsP₃R1 and InsP₃R3 channels described in the accompanying article (Tu et al., 2005). Thus, we have not

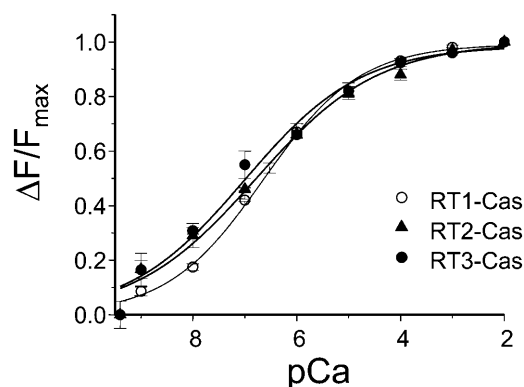


FIGURE 6 Ca²⁺ binding to the InsP₃R Ca²⁺ sensor region. Dilution-corrected and normalized changes in the peak fluorescence intensity ($\Delta F/\Delta F_{\max}$) were averaged together at each Ca²⁺ concentration (see Materials and Methods) and shown as means \pm SE ($n \geq 3$) for RT1-Cas (\circ), RT2-Cas (\blacktriangle), and RT3-Cas (\bullet). The data for each InsP₃R isoform were fitted by Eq. 3 (see Materials and Methods). The parameters of the optimal fits (curves) are presented in Table 1.

induced gross abnormalities in InsP₃R gating and conductance properties by swapping Cas regions between InsP₃R1 and InsP₃R3.

We reasoned that low open probability of RT3-V-1 channels when compared with RT1-V-3 channels in standard recording conditions may be due to lower sensitivity of these channels to ATP modulation, as described for RT3 channels relative to RT1 channels in the accompanying article (Tu et al., 2005). To test this hypothesis, we compared channel activity of RT1-V-3 and RT3-V-1 chimeras in the presence of $2 \mu\text{M}$ InsP₃ at pCa 6.7 in the absence of ATP, at 0.5 mM ATP, and at 5 mM ATP (Fig. 10). We found that both RT1-V-3 and RT3-V-1 channels display very low levels of activity in the absence of ATP ($P_o = 3 \pm 1\%$ ($n = 3$) for RT1-V-3 and $P_o = 2 \pm 1\%$ ($n = 2$) for RT3-V-1) (Fig. 10, A and B, top traces). Addition of 0.5 mM ATP potentiated activity of RT1-V-3 channels to $P_o = 20 \pm 4\%$ ($n = 3$) (Fig. 10 A, middle trace). The P_o of RT3-V-1 channels at 0.5 mM ATP was much lower at $8 \pm 3\%$ ($n = 3$) (Fig. 10 B, middle trace). However, addition of 5 mM ATP resulted in maximal level of activity of both RT1-V-3 ($P_o = 23 \pm 5\%$ ($n = 3$)) and RT3-V-1 ($P_o = 25 \pm 7\%$ ($n = 2$)) channels (Fig. 10, A and B, bottom traces). Comparison with results in the accompanying article (Tu et al., 2005) clearly shows that RT1-V-3 channels are modulated by ATP similar to RT1 channels, and RT3-V-1 channels are modulated by ATP similar to RT3 channels. Thus, the main reason for differences in ATP sensitivity of the RT1 and RT3 channels is related to the presence or absence of the high-affinity ATP site (Fig. 7 A), in agreement with our previous conclusions based on the functional analysis of InsP₃R1-*opt* mutant (Tu et al., 2002).

In the presence of $2 \mu\text{M}$ InsP₃ and 0.5 mM ATP both InsP₃R1 and InsP₃R3 display narrow bell-shaped Ca²⁺

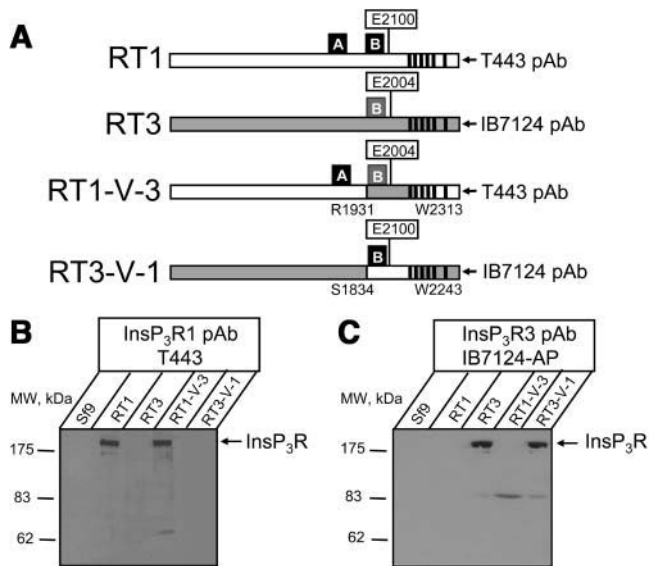


FIGURE 7 Expression of Ca^{2+} sensor swap chimeras. (A) The diagram of RT1, RT3, RT1-V-3, and RT3-V-1 constructs. In RT1-V-3 construct the putative $\text{InsP}_3\text{R1}$ Cas region (E1932-L2312) was replaced by the Cas region of $\text{InsP}_3\text{R3}$ (M1835-F2242; shaded). In RT3-V-1 construct the putative $\text{InsP}_3\text{R3}$ Cas region (M1835-F2242) was replaced by the Cas region of $\text{InsP}_3\text{R1}$ (E1932-L2312; open). Locations of E2100 residue in the $\text{InsP}_3\text{R1}$ Cas sequence (Miyakawa et al., 2001; Tu et al., 2003) and the corresponding E2004 residue in the $\text{InsP}_3\text{R3}$ sequence are shown. Also shown are locations of ATPA ($^{1773}\text{GGGGGGPG}^{1780}$ in $\text{InsP}_3\text{R1}$) and ATPB ($^{2015}\text{GGLGLLG}^{2021}$ in $\text{InsP}_3\text{R1}$ and $^{1919}\text{GGLGLLG}^{1925}$ in $\text{InsP}_3\text{R3}$) sites (Maes et al., 2001) and the epitopes for T443 (anti- $\text{InsP}_3\text{R1}$) (Kaznacheyeva et al., 1998) and IB7124 (anti- $\text{InsP}_3\text{R3}$) (Tu et al., 2005) polyclonal antibodies. (B and C) The microsomes isolated from noninfected Sf9 cells (Sf9), and from Sf9 cells infected with RT1, RT3, RT1-V-3, and RT3-V-1 baculoviruses were analyzed by Western blotting with anti- $\text{InsP}_3\text{R1}$ polyclonal antibody T443 (B) and anti- $\text{InsP}_3\text{R3}$ affinity purified polyclonal antibody IB7124-AP (C). For each microsomal preparation, 10 μg of total protein was loaded on the gel.

dependence with the peak at 257 nM Ca^{2+} for $\text{InsP}_3\text{R1}$ and 107 nM Ca^{2+} for $\text{InsP}_3\text{R3}$ (Fig. 1). To investigate the effects of Cas region swap on sensitivity of InsP_3R to Ca^{2+} , we determined Ca^{2+} dependence of RT1-V-3 and RT3-V-1 channels in the same recording conditions. Because most of the experiments resulted in multichannel bilayers, the P_o values in each experiment were normalized to the maximal P_o in the same experiment as described in Materials and Methods and the normalized data from different experiments with each chimera were averaged together for presentation and analysis. We found that the RT1-V-3 chimera displayed bell-shaped Ca^{2+} dependence that closely overlaps with the RT3 Ca^{2+} dependence with the peak at 100 nM Ca^{2+} (Fig. 11 A, solid circles). Fit to the Ca^{2+} dependence of RT1-V-3 channels using Eq. 1 (Fig. 11 A, smooth thick curve; $R^2 = 0.98$) yielded the apparent affinities of activating and inhibitory Ca^{2+} -binding sites equal to 0.06 ± 0.02 and $0.16 \pm 0.01 \mu\text{M}$ Ca^{2+} (Table 1), identical to the values obtained for the RT3 channels. The difference between RT1-V-3 and RT3 Ca^{2+} -dependence curves was due to differ-

ences in apparent Hill coefficients of Ca^{2+} modulation ($n = 2.17$ for RT1-V-3 and $n = 1.46$ for RT3; Table 1).

In contrast to RT1-V-3, the RT3-V-1 chimera displayed bell-shaped Ca^{2+} dependence that closely overlaps with the RT1 Ca^{2+} dependence with the peak at 239 nM Ca^{2+} (Fig. 11 B). Fit to the Ca^{2+} dependence of RT3-V-1 channels using Eq. 1 (Fig. 11 B, smooth thick curve; $R^2 = 0.99$) yielded the apparent affinities of activating and inhibitory Ca^{2+} -binding sites equal to 0.24 ± 0.01 and $0.25 \pm 0.02 \mu\text{M}$ Ca^{2+} (Table 1), close to the values obtained for the RT1 channels. Similar to RT1-V-3 chimera, the difference between RT3-V-1 and RT1 Ca^{2+} -dependence curves was largely due to differences in apparent Hill coefficients of Ca^{2+} modulation ($n = 1.65$ for RT3-V-1 and $n = 1.23$ for RT1; Table 1). The results obtained with RT1-V-3 and RT3-V-1 chimeras (Fig. 11) indicated that swapping Cas regions between $\text{InsP}_3\text{R1}$ and $\text{InsP}_3\text{R3}$ was sufficient to exchange sensitivities to modulation by Ca^{2+} between these two mammalian InsP_3R isoforms.

In the presence of 5 mM ATP, the RT3 channels display “square-shaped” Ca^{2+} dependence (Fig. 2). In the next series of experiments we compared Ca^{2+} dependence of RT1-V-3 and RT3-V-1 chimeras in the presence of 2 μM InsP_3 and 5 mM ATP. We found that in the presence of 5 mM ATP, RT1-V-3 chimera (Fig. 12, open circles) displayed a “square-shaped” Ca^{2+} dependence very similar to Ca^{2+} dependence of RT3 channels, whereas RT3-V-1 chimera (Fig. 12, triangles) displayed “narrow” Ca^{2+} dependence. Fit to the Ca^{2+} dependence of RT1-V-3 channels using Eq. 2 (Fig. 12, smooth thick curve; $R^2 = 0.98$) yielded the apparent affinities of activating and inhibitory Ca^{2+} -binding sites equal to 0.040 ± 0.003 and $33 \pm 5 \mu\text{M}$ Ca^{2+} (Table 1), close to the values obtained for the RT3 channels at 5 mM ATP. Fit to the Ca^{2+} dependence of RT3-V-1 channels using Eq. 1 (Fig. 12, smooth thick curve; $R^2 = 0.96$) yielded the apparent affinities of activating and inhibitory Ca^{2+} -binding sites equal to 0.28 ± 0.03 and $0.31 \pm 0.04 \mu\text{M}$ Ca^{2+} (Table 1), similar to the values obtained for the RT1 channels.

DISCUSSION

Ca^{2+} dependence of mammalian InsP_3R isoforms

In standard recording conditions (2 μM InsP_3 and 0.5 mM ATP) all three mammalian InsP_3R displayed narrow bell-shaped Ca^{2+} dependence within a physiological range of Ca^{2+} concentrations (pCa 8–5) (Fig. 1; Table 1). In an independent study we demonstrated that *Drosophila melanogaster* InsP_3R displays similar narrow bell-shaped Ca^{2+} dependence when reconstituted into planar lipid bilayers and analyzed in standard recording conditions (Srikanth et al., 2004). Thus, bell-shaped Ca^{2+} dependence of InsP_3R appears to be a fundamental and evolutionary conserved feature of all InsP_3R . This conclusion is in contrast with

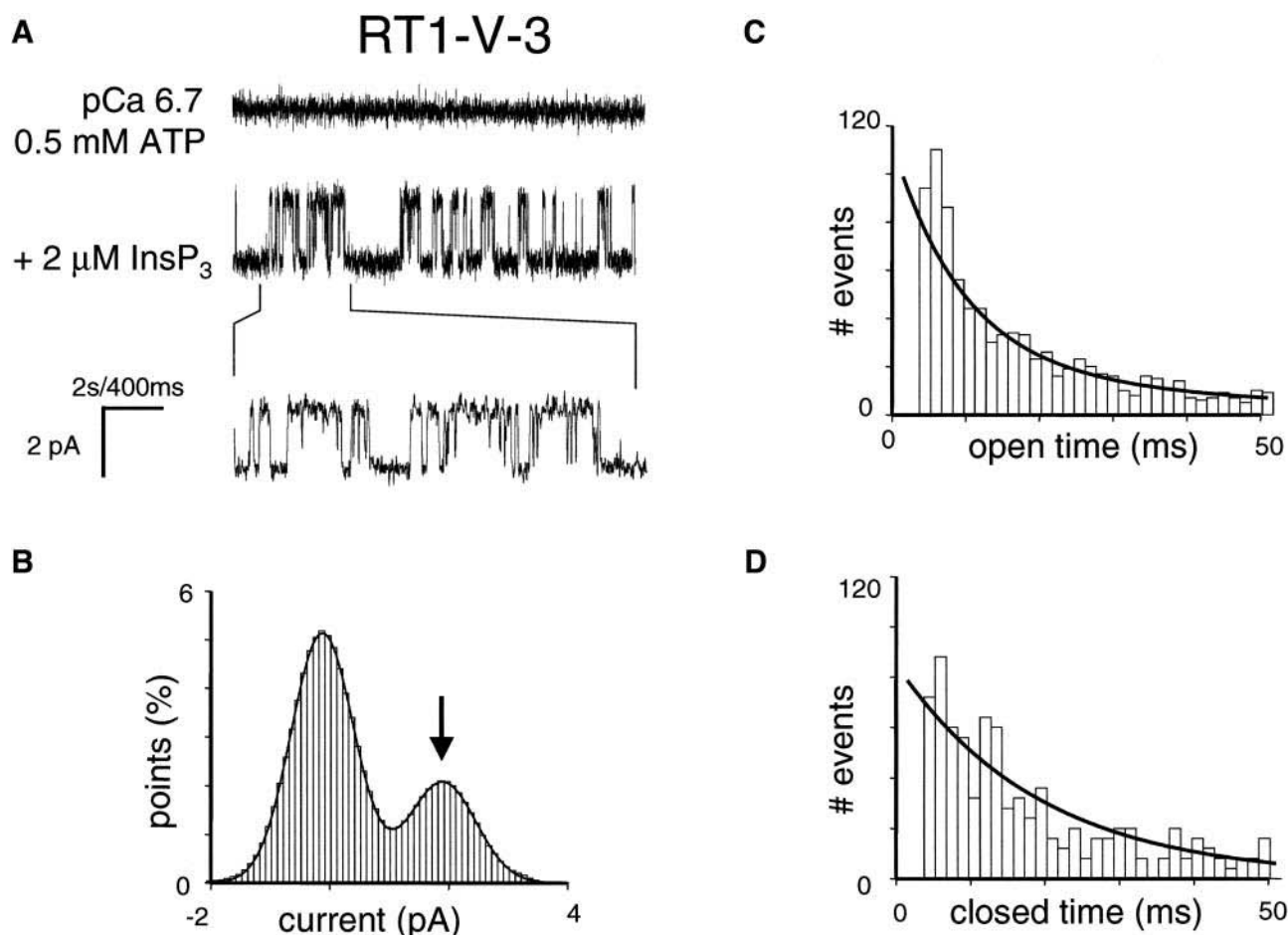


FIGURE 8 Functional properties of RT1-V-3 chimera. (A) Single-channel records of RT1-V-3 channels in planar lipid bilayers. The experiments were performed at pCa 6.7 in the presence of 0.5 mM ATP (control, *top trace*). Addition of 2 μ M InsP₃ to the *cis* (cytoplasmic) side activates RT1-V-3 channels (*middle trace*). Current traces at the expanded timescale are also shown (*bottom trace*). (B–D) Analysis of the single-channel records of RT1-V-3 channels was performed and analyzed as described for InsP₃R1 in the accompanying article (Tu et al., 2005). The Gaussian peak corresponding to an open state of RT1-V-3 was centered at 1.89 pA, had $\sigma = 0.56$ pA, and area 28%. Open time distribution (C; number of events = 2200) was fitted with a single exponential function (*curve*) that yielded mean open time $\tau_o = 8.4$ ms. Closed time distribution (D; number of events = 2200) was fitted with a single exponential function (*curve*) that yielded mean closed time $\tau_c = 9.8$ ms. The data from the same experiment with a single active channel in the bilayer were used for panels A–D.

some previous bilayer studies of InsP₃R2 (Ramos-Franco et al., 2000, 1998) and InsP₃R3 (Hagar et al., 1998). However, bell-shaped Ca²⁺ regulation of InsP₃R3 observed in our experiments is consistent with Ca²⁺ flux measurements in RIN-5F (Swatton et al., 1999) and 16HBE14o-bronchial mucosal cells (Missiaen et al., 1998) and with nuclear patch recordings of recombinant InsP₃R3 expressed in *Xenopus* oocytes (Mak et al., 2001b). The reasons for these discrepancies are not clear. The InsP₃R1 contain a high-affinity Ca²⁺/calmodulin (CaM)-binding site in the coupling domain, which is not conserved in the InsP₃R3 sequence (Yamada et al., 1995). The fact that InsP₃R3 display bell-shaped Ca²⁺ dependence despite the absence of a Ca²⁺/CaM-binding site further supports the notion that association with CaM at this Ca²⁺/CaM binding site does not play a role in biphasic modulation of InsP₃R by Ca²⁺ (Nosyreva et al., 2002; Zhang and Joseph, 2001) (but see Michikawa et al.,

1999). With all three InsP₃R isoforms displaying bell-shaped Ca²⁺ dependence (Fig. 1), how can we explain isoform-specific Ca²⁺ oscillation profiles observed in the study with DT40 cells (Miyakawa et al., 1999)? We would like to suggest that the unique ability of InsP₃R2 to support robust Ca²⁺ oscillations observed in the study of Miyakawa et al. (1999) results from higher affinity of InsP₃R2 for InsP₃ when compared to InsP₃R1 and InsP₃R3 isoforms (Miyakawa et al., 1999; Sudhof et al., 1991; Tu et al., 2005). We would like to suggest that ligation of B-cell receptors (BCR) with anti-BCR antibody in the study with DT40 cells (Miyakawa et al., 1999) resulted in long-lasting InsP₃ elevation above the threshold of InsP₃R2 activation, close to the threshold of InsP₃R1 activation, and below the threshold of InsP₃R3 activation.

The narrow shape of InsP₃R1 bell-shaped Ca²⁺ dependence in our planar lipid bilayer experiments (Fig. 1 and

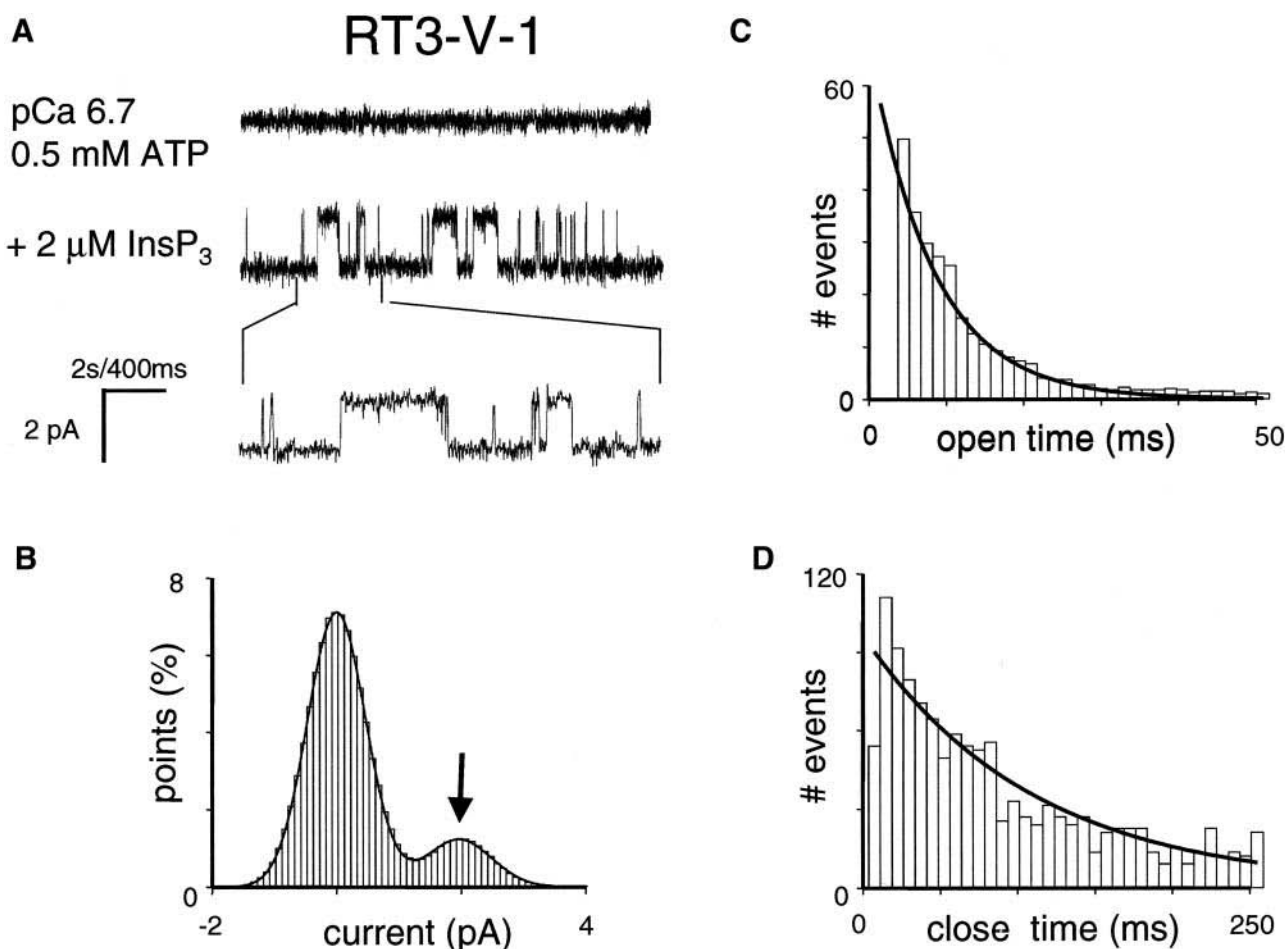


FIGURE 9 Functional properties of RT3-V-1 chimera. (A) Single-channel records of RT3-V-1 channels in planar lipid bilayers. The experiments were performed at pCa 6.7 in the presence of 0.5 mM ATP (control, *top trace*). Addition of 2 μ M InsP₃ to the *cis* (cytoplasmic) side activates RT3-V-1 channels (*middle trace*). Current traces at the expanded timescale are also shown (*bottom trace*). (B–D) Analysis of the single-channel records of RT3-V-1 channels was performed and analyzed as described for InsP₃R3 in the accompanying article (Tu et al., 2005). The Gaussian peak corresponding to an open state of RT3-V-1 was centered at 1.910 pA, had $\sigma = 0.53$ pA, and area 16%. Open and closed time distributions (C and D; number of events = 1000) were fitted with a single exponential function (*curve*) that yielded mean open time $\tau_o = 8.4$ ms and mean closed time $\tau_c = 87.6$ ms for RT3-V-1. The data from the same experiment with a single active channel in the bilayer were used for panels A–D.

Nosyreva et al., 2002; Tu et al., 2002, 2003) is different from the “square” shape described for *Xenopus* InsP₃R (xInsP₃R) (InsP₃R1 homolog; Kume et al., 1993) in nuclear patch experiments by Mak et al. (1998), but it is consistent with the earlier nuclear patch experiments by Stehno-Bittel et al. (1995). Also, the maximal *Po* of InsP₃R1 in our experiments (Tu et al., 2005) and in experiments by Stehno-Bittel et al. (1995) is in the range of 20–30%, whereas *Po* of xInsP₃R in experiments of Mak et al. (1998) reaches 80%. What is an explanation of these differences? And more importantly, what behavior more closely reflects InsP₃R1 function *in vivo*? The *Po* of InsP₃R1 *in vivo* is unknown. However, all Ca²⁺ flux measurements performed with permeabilized cells (Iino, 1990), isolated brain microsomes (Finch et al., 1991), and *Xenopus* oocytes (Parker and Ivorra, 1990; Yao and Parker, 1992) are consistent with the “narrow” shape of

InsP₃R1 Ca²⁺ dependence. In all of these experiments InsP₃-induced Ca²⁺ release was completely blocked by Ca²⁺ concentrations in the 5–10 μ M range, whereas Ca²⁺ concentrations in the 50–100 μ M range were required to inhibit xInsP₃R and InsP₃R3 in nuclear patch recordings of Mak et al. (1998). Therefore, we concluded that “narrow” bell-shaped Ca²⁺ dependence observed in our experiments (Fig. 1 and Nosyreva et al., 2002; Tu et al., 2002, 2003) more closely reflects the physiological behavior of InsP₃R1 and InsP₃R3 than the “square” Ca²⁺ dependence of xInsP₃R reported by Mak et al. (1998).

A recently published mathematical modeling study (Fraiman and Dawson, 2004) offers a potential explanation to the different behavior of InsP₃R1 observed in planar lipid bilayer experiments (Bezprozvanny et al., 1991 and Fig. 1) and in nuclear patch recordings (Mak et al., 1998). Fraiman and

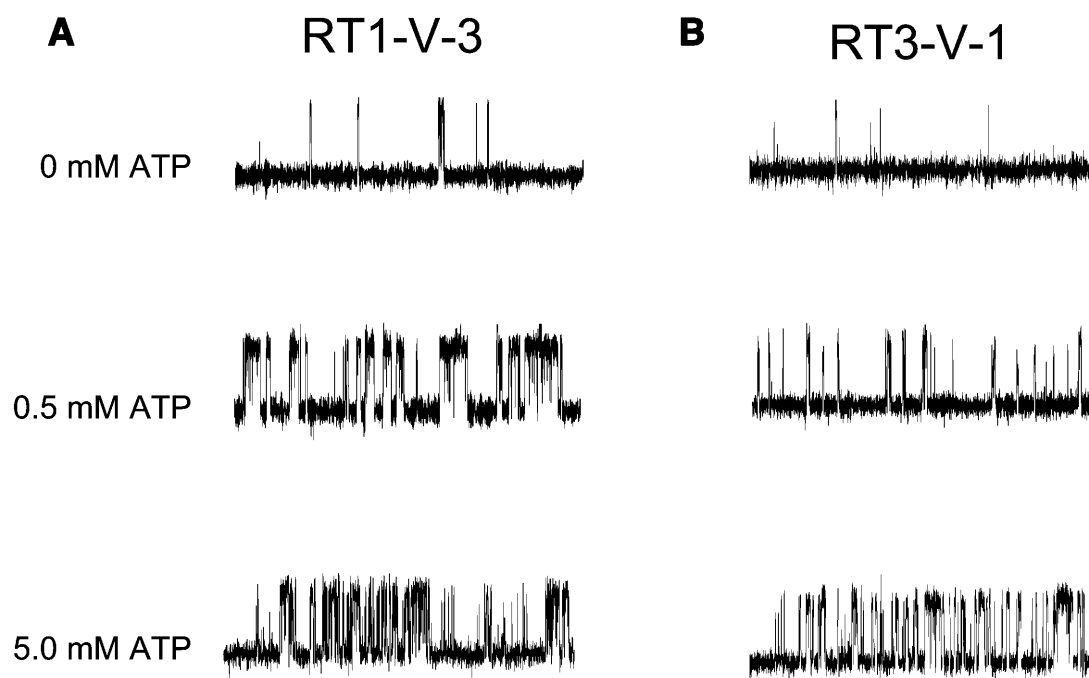


FIGURE 10 ATP sensitivity of Ca²⁺ sensor swap chimeras. Representative current records of RT1-V-3 (A) and RT3-V-1 (B) channels in the bilayers in the presence of 2 μ M InsP₃ and pCa 6.7 at concentrations of Na₂ATP as indicated on the *cis* (cytoplasmic) side of the membrane. The recordings from the same experiment are shown on each panel. Similar results were obtained in at least three experiments with each chimera.

Dawson (2004) were able to explain most of the differences in results obtained in the planar lipid bilayer and nuclear patches recordings of InsP₃R1 activity by introducing an additional intraluminal Ca²⁺ modulatory site. These authors were able to explain “square” Ca²⁺ dependence and high *P_o* of xInsP₃R in nuclear patch recordings of Mak et al. (1998) by the fact that these experiments were performed using monovalent cations to carry current in the absence of Ca²⁺ or other divalent cations. In contrast, the planar lipid bilayer recordings are performed using 50 mM Ca²⁺ (Bezprozvanny et al., 1991) or Ba²⁺ (Fig. 1 and Nosyreva et al., 2002; Tu et al., 2002, 2003) as a current carrier. In the previous study we compared gating of InsP₃R1 with 50 mM Ca²⁺, Ba²⁺, Sr²⁺, and Mg²⁺ as current carriers and analyzed modulation of InsP₃R1 by intraluminal Ca²⁺ levels (Bezprozvanny and Ehrlich, 1994). As discussed by Fraiman and Dawson (2004), the results from Bezprozvanny and Ehrlich (1994) are mostly consistent with the model proposed in their article. Thus, we concluded that “square” Ca²⁺ dependence and high *P_o* of xInsP₃R in nuclear patch recordings of Mak et al. (1998) most likely results from using divalent-free recording conditions (Fraiman and Dawson, 2004). Interestingly, this argument does not explain the difference between results of Mak et al. (1998) and Stehno-Bittel et al. (1995), as both groups used 140 mM K⁺ as a current carrier in nuclear patch recordings of xInsP₃R activity.

In standard recording conditions (2 μ M InsP₃ and 0.5 mM ATP) InsP₃R3 also displayed narrow bell-shaped Ca²⁺

dependence in physiological range of Ca²⁺ concentrations (pCa 8–5) (Fig. 1; Table 1). In contrast to our experiments, Mak et al. reported “square-shaped” Ca²⁺ dependence of rat InsP₃R3 expressed in *Xenopus* oocytes and recorded in nuclear patch experiments in the presence of 0.5 mM ATP and 10 μ M InsP₃ (Mak et al., 2001b). The maximal InsP₃R3 open probability in standard recording conditions in our experiments was low (*P_o* < 5%) (Tu et al., 2005), whereas *P_o* of InsP₃R3 in experiments of Mak et al. (2001b) reaches 80%. Once again, “narrow” bell-shaped Ca²⁺ dependence of InsP₃R3 is consistent with Ca²⁺ flux measurements in permeabilized 16HBE14o- bronchial mucosal cells and RINm5F cells enriched in InsP₃R3 (Missiaen et al., 1998; Swatton et al., 1999). The explanation of the differences between “narrow” and “square-shaped” Ca²⁺ dependence of InsP₃R3 observed in our experiments (Fig. 1) and in experiments of Mak et al. (2001b) is most likely related to use of divalent-free recording conditions as discussed above for InsP₃R1.

Interestingly, the “narrow” Ca²⁺ dependence of InsP₃R3 in standard recording conditions (2 μ M InsP₃ and 0.5 mM ATP) (Fig. 1) was converted to “square-shaped” Ca²⁺ dependence when recordings were performed in the presence of 2 μ M InsP₃ and 5 mM ATP (Fig. 2). The ATP-induced change in the shape of Ca²⁺ dependence was a unique feature of InsP₃R3, as Ca²⁺ dependence of InsP₃R1 remained “narrow” in the presence of 5 mM ATP (data not shown). Fit to “narrow” (Fig. 1) and “square” (Fig. 2)

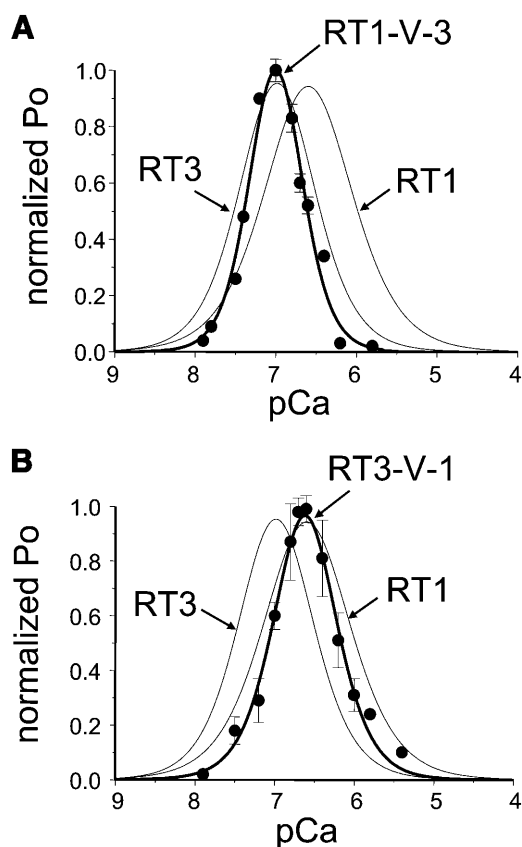


FIGURE 11 Ca^{2+} dependence of Ca^{2+} sensor swap chimeras at 0.5 mM ATP. Ca^{2+} dependence of RT1-V-3 (A) and RT3-V-1 (B) chimeras in planar lipid bilayers. The normalized and averaged data (see Materials and Methods) at each Ca^{2+} concentration are shown as means \pm SE ($n \geq 3$) (●). The data were fit (thick lines) by Eq. 1 (see Materials and Methods). The parameters of the best fits are in Table 1. The fits to $\text{InsP}_3\text{R1}$ and $\text{InsP}_3\text{R3}$ (at 0.5 mM ATP) Ca^{2+} dependence curves (thin lines) are from Fig. 1.

Ca^{2+} -dependence curves of $\text{InsP}_3\text{R3}$ indicated that an increase in ATP concentration from 0.5 to 5 mM resulted in a twofold increase in the apparent affinity of the Ca^{2+} -activating site of $\text{InsP}_3\text{R3}$ and a >200 -fold reduction in the apparent affinity of the Ca^{2+} -inhibitory site of $\text{InsP}_3\text{R3}$ (Table 1). In experiments of Mak et al. (2001a) with $\text{InsP}_3\text{R3}$ expressed in *Xenopus* oocytes an increase in ATP concentration from 0 to 0.5 mM resulted in a 10-fold increase in the affinity of the Ca^{2+} -activating site and a threefold increase in the affinity of the Ca^{2+} -inhibitory site. Unfortunately, the inhibitory phase of $\text{InsP}_3\text{R3}$ Ca^{2+} dependence was not analyzed at ATP concentrations >0.5 mM by Mak et al. (2001a), so it is not clear if the differences between our studies and the Mak et al. studies are due to a different range of ATP concentrations compared (0.5 and 5 mM in our study and 0 and 0.5 mM in the Mak et al., 2001a study) or because of the use of divalent-free recording conditions as discussed above. Notably, Mak et al. (1998) earlier reported that the increase in InsP_3 concentration from 20 nM to 10 μM leads to a 280-fold reduction in the apparent affinity of the Ca^{2+} -

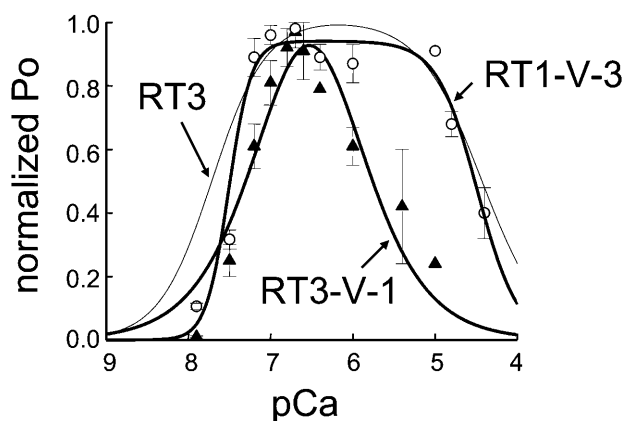


FIGURE 12 Ca^{2+} dependence of Ca^{2+} sensor swap chimeras at 5 mM ATP. Ca^{2+} dependence of RT1-V-3 (○) and RT3-V-1 (▲) chimeras in planar lipid bilayers at the presence of 5 mM ATP. The normalized and averaged data (see Materials and Methods) at each Ca^{2+} concentration are shown as means \pm SE ($n \geq 3$). The RT1-V-3 data were fit by Eq. 2 (thick curve) and the RT3-V-1 data were fit by Eq. 1 (thick curve). The parameters of the best fits are in Table 1. The fit to Ca^{2+} dependence of $\text{InsP}_3\text{R3}$ at 5 mM ATP (thin line) is from Fig. 2.

inhibitory site of xInsP_3R . In our hands the affinity of the $\text{InsP}_3\text{R3}$ Ca^{2+} -inhibitory site is affected in a very similar way by an increase in ATP concentration (Figs. 1 and 2; Table 1).

The role of InsP_3R Ca^{2+} sensor

When modulation of different InsP_3R isoforms by Ca^{2+} was compared side-by-side in standard recording conditions (2 μM InsP_3 and 0.5 mM ATP), we discovered that $\text{InsP}_3\text{R3}$ are most sensitive to modulation by Ca^{2+} (peak at 107 nM Ca^{2+}), followed by $\text{InsP}_3\text{R2}$ (peak at 154 nM Ca^{2+}), and then by $\text{InsP}_3\text{R1}$ (peak at 257 nM Ca^{2+}) (Fig. 1; Table 1). High sensitivity to activation by Ca^{2+} observed for $\text{InsP}_3\text{R2}$ is consistent with the previous Ca^{2+} flux studies in DT40 cells (Miyakawa et al., 1999) and with the single-channel recordings of native and recombinant $\text{InsP}_3\text{R2}$ (Ramos-Franco et al., 2000, 1998). High sensitivity to activation by Ca^{2+} observed for $\text{InsP}_3\text{R3}$ is also consistent with previous Ca^{2+} flux studies in DT40 cells (Miyakawa et al., 1999) and with single-channel recordings of recombinant $\text{InsP}_3\text{R3}$ expressed in *Xenopus* oocytes (Mak et al., 2001b).

In the previous studies (Miyakawa et al., 2001; Tu et al., 2003) we identified a putative Ca^{2+} sensor (Cas) region in the $\text{InsP}_3\text{R1}$ sequence. The sequence of Cas region is highly conserved between InsP_3R isoforms (Fig. 4), including a conserved glutamate residue (E2100 in $\text{InsP}_3\text{R1}$), the importance of which we established previously (Miyakawa et al., 2001; Tu et al., 2003). Are small variations in Cas sequence (Fig. 4) sufficient to explain different Ca^{2+} sensitivity of InsP_3R isoforms? To answer this question, we expressed RT1-Cas, RT2-Cas, and RT3-Cas proteins in

bacteria (Fig. 3) and performed a series of intrinsic tryptophan fluorescence measurements at different Ca²⁺ concentrations by following a method described previously for RT1-Cas (Tu et al., 2003). Importantly, the W2255 and W2267 residues of InsP₃R1 present within the RT1-Cas region (Fig. 4, *open arrows*) are conserved in InsP₃R2 and InsP₃R3. For all three RT-Cas proteins, the intensity of the intrinsic tryptophan fluorescence signal was quenched as a function of Ca²⁺ (Fig. 5), consistent with Ca²⁺-induced conformational change. By fitting the obtained results we determined that the RT1-Cas apparent affinity for Ca²⁺ (K_{Ca}) is equal to 0.23 μ M, RT2-Cas apparent affinity for Ca²⁺ is equal to 0.16 μ M, and RT3-Cas apparent affinity for Ca²⁺ is equal to 0.10 μ M (Fig. 6; Table 1). Thus, small variations in Cas sequence between different InsP₃R isoforms (Fig. 4) do appear to be sufficient to result in different affinities for Ca²⁺ (Fig. 6). Future mutagenesis of the RT-Cas region or solution of the RT-Cas structure will be required to identify structural determinants that form a Ca²⁺-binding site within the RT-Cas region.

Ca²⁺ binding affinities of isolated RT-Cas regions are in quantitative agreement with the sensitivity of corresponding InsP₃R isoforms to the Ca²⁺ modulation determined in planar lipid bilayer experiments (Table 1). Are different RT-Cas affinities for Ca²⁺ sufficient to explain different Ca²⁺ sensitivity of InsP₃R isoforms? To answer this question, we swapped Cas regions between the InsP₃R1 and InsP₃R3 isoforms and generated baculoviruses encoding RT1-V-3 and RT3-V-1 chimeras (Fig. 7). Single-channel analysis revealed that conductance and gating properties of RT1-V-3 and RT3-V-1 chimeras are similar to the properties of “parental channels” (Figs. 8 and 9). Thus, swapping InsP₃R1 and InsP₃R3 Cas regions did not induce gross abnormalities in InsP₃R gating and conductance properties. The low-affinity ATP-binding site (ATPB) is contained within the Cas region (Fig. 4). Thus, RT1-V-3 chimera contains the ATPA site from InsP₃R1 and the ATPB site from InsP₃R3 (Fig. 7 A), and RT3-V-1 chimera contains the ATPB site from InsP₃R1 (Fig. 7 A). Consistent with the predominant role played by the ATPA site in modulating InsP₃R1 gating by ATP (Maes et al., 2001; Tu et al., 2002), RT1-V-3 chimera displayed ATP sensitivity similar to InsP₃R1 (Fig. 10 A) and RT3-V-1 chimera displayed ATP sensitivity similar to InsP₃R3 (Fig. 10 B).

Consistent with “Ca²⁺ sensor hypothesis,” we found that swapping Cas regions was sufficient to exchange Ca²⁺ sensitivities of InsP₃R1 and InsP₃R3 isoforms (Fig. 11, A and B; Table 1). Interestingly, both activating and inhibitory parts of bell-shaped Ca²⁺ dependence were affected by Cas domain swap in our experiments with RT1-V-3 and RT3-V-1 chimeras (Fig. 11, A and B). These results are consistent with our previous analysis of RT1-E2100 point mutants (Tu et al., 2003). As discussed in Tu et al. (2003), these data can be explained if Cas region forms a part of both Ca²⁺-activating and Ca²⁺-inhibitory sites, or by sequential Ca²⁺

binding to activating and inhibitory sites of the InsP₃R. In our experiments we found that the Ca²⁺ sensitivity of RT1-V-3 chimera closely resembles Ca²⁺ sensitivity of RT3 (Fig. 11 A), and the Ca²⁺ sensitivity of RT3-V-1 chimera closely matches Ca²⁺ sensitivity of RT1 (Fig. 11 B). Moreover, at 5 mM ATP RT1-V-3 chimera displayed “square-shaped” Ca²⁺ dependence similar to RT3, whereas RT3-V-1 chimera displayed “narrow” Ca²⁺ dependence similar to RT1 (Fig. 12). These results indicate that the features responsible for ATP-dependent transition from “narrow” to “square” Ca²⁺ dependence are uniquely encoded within RT3-Cas sequence.

Our results with RT1-V-3 and RT3-V-1 chimeras are in contrast to recent analysis of InsP₃R1/2 and InsP₃R2/1 coupling domain swap chimeras (Ramos et al., 2003). In the study of Ramos et al. (2003) Ca²⁺ sensitivity of 1-2-1 and 2-1-2 chimeras was largely lost and did not resemble Ca²⁺ sensitivity of either “parental” InsP₃R (type 1 or type 2). Most likely explanation for the differences between our results and the results of Ramos et al. (2003) is related to the choice of boundaries for “domain swap”. In our RT1-V-3 and RT3-V-1 constructs we choose domain swap boundaries (E1932 in InsP₃R1 and M1835 in InsP₃R3, Figs. 4 and 7 A) from the limited trypsin digestion pattern of InsP₃R1 (Yoshikawa et al., 1999), which also corresponds to the region of sequence divergence between InsP₃R isoforms. In contrast, Ramos et al. (2003) choose the most conserved regions of the InsP₃R1 and InsP₃R2 sequences as boundaries for the coupling domain swap in 1-2-1 and 2-1-2 chimeras. Indeed, we obtained functional results similar to that of Ramos et al. (2003) with several other InsP₃R3/1 chimeric constructs with domain swap boundaries chosen in conserved regions of InsP₃R1 and InsP₃R3 sequences (data not shown).

Common and unique properties of mammalian InsP₃R isoforms

In summary, data presented in this and the accompanying article (Tu et al., 2005) as well as the majority of the previously published reports indicate that all three mammalian InsP₃R isoforms share common gating and conductance properties and display bell-shaped sensitivity to Ca²⁺ in a physiological range of Ca²⁺ concentrations (pCa 8–5). When compared to each other, the InsP₃R1 is a medium InsP₃-affinity, high ATP-affinity (no cooperativity), and low Ca²⁺-affinity isoform; the InsP₃R2 is a high InsP₃-affinity, ATP-independent, medium Ca²⁺-affinity isoform; the InsP₃R3 is a low InsP₃-affinity, low ATP-affinity (high cooperativity), and high Ca²⁺-affinity isoform. Interestingly, saturation of the ATP binding site of InsP₃R3 (but not InsP₃R1) reduces apparent affinity of the Ca²⁺-inhibitory site by >200-fold and converts “narrow” bell-shaped Ca²⁺ dependence of InsP₃R3 (Fig. 1) to “square” Ca²⁺ dependence (Fig. 2). It appears that high affinity of InsP₃R2 for

InsP₃ is encoded within the amino-terminal ligand-binding domain (Sudhof et al., 1991), high affinity of InsP₃R1 for ATP is due to the high-affinity ATPA binding site in the InsP₃R1 sequence (Fig. 10; also Maes et al., 2001; Tu et al., 2002), and the differences in Ca²⁺ sensitivity are encoded within a sequence of Ca²⁺ sensor (Cas) region (Figs. 4, 6, 11, and 12). These conclusions will be useful for understanding the mechanisms of InsP₃R function and for analysis of Ca²⁺ signals supported by various InsP₃R subtypes expressed in cells and tissues.

We are grateful to Gregory Mignery and Thomas C. Südhof for the kind gift of the rat InsP₃R1 and InsP₃R2 clones, to Graeme Bell for the kind gift of the rat InsP₃R3 clone, and to Humbert De Smedt for RT3 baculovirus. We thank Phyllis Foley for the administrative assistance and Elena Nosyreva for help with bilayer experiments.

This work was supported by the Welch Foundation and National Institutes of Health (R01 NS38082 to I.B.).

REFERENCES

- Berridge, M. J. 1993. Inositol trisphosphate and calcium signalling. *Nature*. 361:315–325.
- Bezprozvanny, I., and B. E. Ehrlich. 1994. Inositol (1,4,5)-trisphosphate (InsP₃)-gated Ca channels from cerebellum: conduction properties for divalent cations and regulation by intraluminal calcium. *J. Gen. Physiol.* 104:821–856.
- Bezprozvanny, I., J. Watras, and B. E. Ehrlich. 1991. Bell-shaped calcium-response curves of Ins(1,4,5)P₃- and calcium-gated channels from endoplasmic reticulum of cerebellum. *Nature*. 351:751–754.
- Fabiato, A. 1988. Computer programs for calculating total from specified free or free from specified total ionic concentrations in aqueous solutions containing multiple metals and ligands. *Methods Enzymol.* 157:378–417.
- Finch, E. A., T. J. Turner, and S. M. Goldin. 1991. Calcium as a coagonist of inositol 1,4,5-trisphosphate-induced calcium release. *Science*. 252:443–446.
- Fraiman, D., and S. P. Dawson. 2004. A model of the IP₃ receptor with a luminal calcium binding site: stochastic simulations and analysis. *Cell Calcium*. 35:403–413.
- Furuichi, T., K. Kohda, A. Miyawaki, and K. Mikoshiba. 1994. Intracellular channels. *Curr. Opin. Neurobiol.* 4:294–303.
- Hagar, R. E., A. D. Burgstahler, M. H. Nathanson, and B. E. Ehrlich. 1998. Type III InsP₃ receptor channel stays open in the presence of increased calcium. *Nature*. 396:81–84.
- Iino, M. 1990. Biphasic Ca²⁺ dependence of inositol 1,4,5-trisphosphate-induced Ca release in smooth muscle cells of the guinea pig *Taenia caeci*. *J. Gen. Physiol.* 95:1103–1122.
- Kaznatcheyeva, E., V. D. Lupu, and I. Bezprozvanny. 1998. Single-channel properties of inositol (1,4,5)-trisphosphate receptor heterologously expressed in HEK-293 cells. *J. Gen. Physiol.* 111:847–856.
- Kume, S., A. Muto, J. Aruga, T. Nakagawa, T. Michikawa, T. Furuichi, S. Nakade, H. Okano, and K. Mikoshiba. 1993. The *Xenopus* IP₃ receptor: structure, function, and localization in oocytes and eggs. *Cell*. 73:555–570.
- Maes, K., L. Missiaen, P. De Smet, S. Vanlingen, G. Callewaert, J. B. Parys, and H. De Smedt. 2000. Differential modulation of inositol 1,4,5-trisphosphate receptor type 1 and type 3 by ATP. *Cell Calcium*. 27:257–267.
- Maes, K., L. Missiaen, J. B. Parys, P. De Smet, I. Sienaert, E. Waelkens, G. Callewaert, and H. De Smedt. 2001. Mapping of the ATP-binding sites on inositol 1,4,5-trisphosphate receptor type 1 and type 3 homotetramers by controlled proteolysis and photoaffinity labeling. *J. Biol. Chem.* 276:3492–3497.
- Mak, D. O., S. McBride, and J. K. Foskett. 1998. Inositol 1,4,5-trisphosphate activation of inositol trisphosphate receptor Ca²⁺ channel by ligand tuning of Ca²⁺ inhibition. *Proc. Natl. Acad. Sci. USA*. 95:15821–15825.
- Mak, D. O., S. McBride, and J. K. Foskett. 2001a. ATP regulation of recombinant type 3 inositol 1,4,5-trisphosphate receptor gating. *J. Gen. Physiol.* 117:447–456.
- Mak, D. O., S. McBride, and J. K. Foskett. 2001b. Regulation by Ca²⁺ and inositol 1,4,5-trisphosphate (InsP₃) of single recombinant type 3 InsP₃ receptor channels. Ca²⁺ activation uniquely distinguishes types 1 and 3 InsP₃ receptors. *J. Gen. Physiol.* 117:435–446.
- Michikawa, T., J. Hirota, S. Kawano, M. Hiraoka, M. Yamada, T. Furuichi, and K. Mikoshiba. 1999. Calmodulin mediates calcium-dependent inactivation of the cerebellar type 1 inositol 1,4,5-trisphosphate receptor. *Neuron*. 23:799–808.
- Missiaen, L., J. B. Parys, I. Sienaert, K. Maes, K. Kunzelmann, M. Takahashi, K. Tanzawa, and H. De Smedt. 1998. Functional properties of the type-3 InsP₃ receptor in 16HBE14o- bronchial mucosal cells. *J. Biol. Chem.* 273:8983–8986.
- Miyakawa, T., A. Maeda, T. Yamazawa, K. Hirose, T. Kurosaki, and M. Iino. 1999. Encoding of Ca²⁺ signals by differential expression of IP₃ receptor subtypes. *EMBO J.* 18:1303–1308.
- Miyakawa, T., A. Mizushima, K. Hirose, T. Yamazawa, I. Bezprozvanny, T. Kurosaki, and M. Iino. 2001. Ca(2+)-sensor region of IP(3) receptor controls intracellular Ca(2+) signaling. *EMBO J.* 20:1674–1680.
- Nosyreva, E., T. Miyakawa, Z. Wang, L. Glouchankova, A. Mizushima, M. Iino, and I. Bezprozvanny. 2002. The high affinity calcium-calmodulin-binding site does not play a role in modulation of type 1 inositol (1,4,5)-trisphosphate receptor function by calcium and calmodulin. *Biochem. J.* 365:659–667.
- Parker, I., and I. Ivorra. 1990. Inhibition by Ca²⁺ of inositol trisphosphate-mediated Ca²⁺ liberation: a possible mechanism for oscillatory release of Ca²⁺. *Proc. Natl. Acad. Sci. USA*. 87:260–264.
- Ramos, J., W. Jung, J. Ramos-Franco, G. A. Mignery, and M. Fill. 2003. Single channel function of inositol 1,4,5-trisphosphate receptor type-1 and -2 isoform domain-swap chimeras. *J. Gen. Physiol.* 121:399–411.
- Ramos-Franco, J., D. Bare, S. Caenepeel, A. Nani, M. Fill, and G. Mignery. 2000. Single-channel function of recombinant type 2 inositol 1,4,5-trisphosphate receptor. *Biophys. J.* 79:1388–1399.
- Ramos-Franco, J., M. Fill, and G. A. Mignery. 1998. Isoform-specific function of single inositol 1,4,5-trisphosphate receptor channels. *Biophys. J.* 75:834–839.
- Srikanth, S., Z. Wang, H. Tu, S. Nair, M. K. Mathew, G. Hasan, and I. Bezprozvanny. 2004. Functional properties of the *Drosophila melanogaster* inositol 1,4,5-trisphosphate receptor mutants. *Biophys. J.* 86:3634–3646.
- Stehno-Bittel, L., A. Luckhoff, and D. E. Clapham. 1995. Calcium release from the nucleus by InsP₃ receptor channels. *Neuron*. 14:163–167.
- Sudhof, T. C., C. L. Newton, B. T. Archer, Y. A. Ushkaryov, and G. A. Mignery. 1991. Structure of a novel InsP₃ receptor. *EMBO J.* 10:3199–3206.
- Swatton, J. E., S. A. Morris, T. J. Cardy, and C. W. Taylor. 1999. Type 3 inositol trisphosphate receptors in RINm5F cells are biphasically regulated by cytosolic Ca²⁺ and mediate quantal Ca²⁺ mobilization. *Biochem. J.* 344:55–60.
- Taylor, C. W., A. A. Genazzani, and S. A. Morris. 1999. Expression of inositol trisphosphate receptors. *Cell Calcium*. 26:237–251.
- Tu, H., T. Miyakawa, Z. Wang, L. Glouchankova, M. Iino, and I. Bezprozvanny. 2002. Functional characterization of the type 1 inositol 1,4,5-trisphosphate receptor coupling domain SII(+/-) splice variants and the *Opisthotonos* mutant form. *Biophys. J.* 82:1995–2004.
- Tu, H., E. Nosyreva, T. Miyakawa, Z. Wang, A. Mizushima, M. Iino, and I. Bezprozvanny. 2003. Functional and biochemical analysis of the type 1 inositol (1,4,5)-trisphosphate receptor calcium sensor. *Biophys. J.* 85:290–299.

- Tu, H., Z. Wang, E. Nosyreva, H. De Smedt, and I. Bezprozvanny. 2005. Functional characterization of mammalian inositol 1,4,5-trisphosphate receptor isoforms. *Biophys. J.* 88:1046–1055.
- Ward, L. D. 1985. Measurement of ligand binding to proteins by fluorescence spectroscopy. *Methods Enzymol.* 117:400–414.
- Yamada, M., A. Miyawaki, K. Saito, T. Nakajima, M. Yamamoto-Hino, Y. Ryo, T. Furuichi, and K. Mikoshiba. 1995. The calmodulin-binding domain in the mouse type 1 inositol 1,4,5-trisphosphate receptor. *Biochem. J.* 308:83–88.
- Yao, Y., and I. Parker. 1992. Potentiation of inositol trisphosphate-induced Ca²⁺ mobilization in *Xenopus* oocytes by cytosolic Ca²⁺. *J. Physiol.* 458:319–338.
- Yoshikawa, F., H. Iwasaki, T. Michikawa, T. Furuichi, and K. Mikoshiba. 1999. Trypsinized cerebellar inositol 1,4,5-trisphosphate receptor. Structural and functional coupling of cleaved ligand binding and channel domains. *J. Biol. Chem.* 274:316–327.
- Zhang, X., and S. K. Joseph. 2001. Effect of mutation of a calmodulin binding site on Ca²⁺ regulation of inositol trisphosphate receptors. *Biochem. J.* 360:395–400.